Local variations of air velocity in the vicinity of filter pleats in transitional airflow regime – Experimental and numerical approaches

Walid Mrad, Félicie Theron, Aurélie Joubert, Nancy Zgheib, Laurence Le Coq

Version of Record: https://www.sciencedirect.com/science/article/pii/S1383586621003701
Manuscript_fb4da31ce342083dca83a7bc7b15cffb

Local variations of air velocity in the vicinity of filter pleats in transitional airflow regime - experimental and numerical approaches

Walid Mrad[1], Félicie Theron[1*], Aurélie Joubert[1], Nancy Zgheib[2], Laurence Le Coq[1]

[1] IMT Atlantique, CNRS, GEPEA, UMR 6144, 4 rue Alfred Kastler, F-44307 Nantes, France
[2]USEK, CNRS-L, AUF Kaslik, Jounieh, Lebanon
*Corresponding author: felicie.theron@imt-atlantique.fr

ABSTRACT

This study combines experimental velocity measurements and numerical simulations to characterize the airflow in the vicinity of pleated filters used in ventilation systems. Experimental velocity and turbulence intensity profiles were measured using Hot Wire Anemometry (HWA), upstream and downstream of the filter. Significant local velocity gradients were detected downstream of the filter. The maximum local velocity detected was as much as three times the inlet velocity. The gradient was constant up to 2.5 cm from the pleat entrance. However, only slight velocity variations were observed upstream of the filter. Computational Fluid Dynamics (CFD) simulations were performed using the Ansys Fluent code. Since the flow regime of the airflow approaching filters was transitional, the three following flow models were tested: laminar, standard k-ε, and transition SST. The numerical velocity data were in fairly close agreement with the experimental velocity profiles upstream and downstream of the filter, especially in close proximity to the filter medium. No significant turbulence intensities were detected close to the medium surface for the filtration velocity tested.

Keywords: air filtration, filter pleats, airflow pattern, CFD calculation, Hot Wire Anemometry.

1. Introduction

For several years, air quality has become a major issue for public opinion as well as for the scientific, industrial and political communities, who wish to reduce exposure to particles that are potentially hazardous to human health. Regarding the removal of particulate matter from buildings, filters made of fibrous media are the most commonly used in air treatment systems, as one-stage or two-stage filters. However, the significant pressure drop they generate and the maintenance costs caused by clogging remain challenging. HVAC (Heating Ventilation Air Conditioning) systems account for about 60% of the total energy cost of buildings [1].
The design of fibrous filters requires selection of a relevant fibrous medium to achieve the targeted efficiency, and determination of relevant geometric properties to minimize pressure drop and consequently energy consumption. Introducing a fibrous medium in a geometrically-pleated design increases the available filtration surface, but also causes significant local velocity gradients and possibly local efficiency gradients, which may affect the average performance. The velocity at which particles reach the fibrous medium is referred in the literature as the filtration velocity. This is calculated as the ratio of the airflow rate approaching the filter and the developed filter medium surface. This velocity is one of the critical parameters affecting filtration performances, especially particle collection efficiency. A high filtration velocity value tends to decrease particle collection by Brownian diffusion and increase collection by the inertial impaction mechanism. The study of airflow in the vicinity of fibrous filters with complex geometrical properties such as pleated filters is therefore crucial for precise evaluation of its possible influence on filtration performances, on which filter design is based.

Many studies reported in the literature deal with improving the filtration performances of pleated filters (i.e. reducing the pressure drop while maintaining the targeted filtration efficiency) by combining semi-empirical models with numerical simulations. To this end, the main challenge encountered by the authors has been to take into consideration the airflow pattern approaching the pleated filter. Although some studies presented in the literature detected velocity gradients in the pleat channel, these were not included when calculating the collection efficiency. Instead they concentrated on the filtration velocity, which does not reflect the local conditions experienced by the particles and therefore affects the accuracy of the models. Terrill et al. [2] introduced the theoretical study of airflow in uniform channels bounded by porous walls. By using 'similarity' equations, they simplified the Navier-Stokes (NS) equations in partial differential equations, which can be solved using simple numerical algorithms. This work has been taken up in filtration studies by Oxarango et al. [3] and more recently Rebaï et al. [4], who developed a semi-analytical model allowing prediction of the pressure drop and velocity field in rectangular and triangular pleats. They showed that velocity does not remain constant along the pleat depth, which may cause preferential zones for the deposition of particles at the bottom of channels. However, this model is sensitive to the geometric and structural properties of the pleat bottom and is applicable only for high filtration velocities. Other purely numerical investigations have been carried out along these lines [5-10]. More details concerning the conditions for these numerical studies have been recapitulated by Theron et al. [11]. The literature also includes many numerical studies dealing with the effect of the filter's geometrical properties on the velocity pattern in the vicinity of the filter [4,5,11-17]. Most of these studies focus on airflow behavior upstream of the pleat channel, since this is the primary interest regarding particle collection.

With all the numerical calculations mentioned above, the difficulty arises in selecting an appropriate airflow model to simulate the airflow approaching the filter. In the literature, validation of the airflow model is almost always based on the pressure drop, which is a macroscopic parameter [11,18]. Few studies have validated their numerical approach using local parameters such as velocity values. This is probably due to the fact that measuring local velocity values in close proximity to filters represents a challenging issue for the experiment. The most commonly-used techniques for this purpose are Hot Wire Anemometry (HWA) [15,18] and Particle Image Velocimetry (PIV) [15]. With PIV, the tracer particles can deviate from the air streamline and be collected by the filter. So they are no longer representative of the airflow in the vicinity of the medium and can increase the pressure drop. Unlike PIV [15], HWA does not require tracer particles. Another advantage of HWA is its ability to measure velocity fluctuations in addition to local velocity magnitude, and also turbulent characteristics like Reynolds stresses and vorticity [19]. HWA is therefore a suitable technique for this study. Feng et al. [18], for example, measured the one-dimensional longitudinal velocity component using HWA downstream of a rectangular-shaped filter (height H = 50 mm, width W = 50 mm). They measured transversal velocity profiles inside and outside the pleat. They were able to get as close as 3 mm from the filter surface. Maddineni et al. [14] used the same technique to measure transversal velocity profiles upstream, on the outside of a mini-pleated geometry filter (H = 26 mm, W = 4.5 mm). Since they were not able to go inside the filter due to the restricted space available, the HWA probe was 3.1 mm away from the pleat entrance. Kang et al. [15] used PIV to measure the velocity downstream of a custom-built rectangular pleat (H = 51 mm, W = 51 mm). Their results showed significant velocity gradients downstream of the pleat. The importance of the velocity gradient downstream of the pleat on filtration performances is barely tackled in the literature, despite the potential importance of optimizing filtration performances, especially for indoor air applications where filters are installed in series. The non-uniform

velocity distribution generated by a pre-filter can actually affect the efficiency and life span of the filter. A recent numerical study by Maddineni et al. [20] showed that a high filtration velocity could amplify penetration through the filter by causing particle bounce and re-entrainment downstream of the filter. To ensure better optimization of filter performances during clogging, therefore, special attention should be given to flow behavior on both sides of the pleat.

This study combines experimental velocity measurements using HWA and numerical simulations in the vicinity of filter pleats, in order to investigate the local velocity gradients upstream and downstream of a pleated filter with geometrical properties representative of those used in air handling units. The first part of the paper introduces the filter properties and experiment conditions. The influence of filter geometry and medium permeability on the simulated pressure drop is then investigated and compared with the experimental results. Next, experimental velocity profiles upstream and downstream of the filter pleats are presented and compared to the results of the numerical simulations. After having validated the CFD, further numerical investigations of the velocity at the air/filter interface are conducted. Finally, the experimental local turbulence intensity values acquired by the HWA technique in the vicinity of the filter pleats are presented.

2. Materials and method

2.1 Studied filter

The filter studied was made of a fibrous medium manufactured by the Lydall© Company, widely used for indoor air treatment applications. It has an efficiency expressed as ISO ePM1 50-55% according to ISO16890 standards. 94% of the fibers are made of glass and 2% are synthetic. The rest are acrylic fiber binders and hydrophobic additives. The properties of the medium and the experiment techniques used to characterize them are summarized in Table 1. To carry out experimental measurements of pressure drop and velocity, three downsized pleated-filter prototypes were manufactured in the laboratory. These had six pleats of 28 ± 1 mm height and 25 ± 1 mm width, and a filtration surface of 55,200 ± 2,000 mm².

Table 1 Properties of medium.
*Measurements carried out at the facility, developed at the LGP2 laboratory and used by Zerrouati et al [21].
+Measurement of pressure drop generated by the fibrous medium (in flat configuration) as a function of air velocity, for an air velocity range of 0 – 1.56 $m.s^{-1}$

Property	Values	Measurement technique
Thickness	601 ± 19 µm (11 samples)	Low-pressure measurement*
Mean fiber diameter	3.14 ± 2.09 µm (950 fibers counted)	SEM (JEOL JSM 7600F) and picture analysis using Image J
Permeability	$(3.10 \pm 0.10).10^{-11}$ m² (3 samples)	Permeametry+
Mean porosity	92 ± 2 % (3 samples)	Mercury porosimetry (Micrometrics Autoport IV)
Mean pore diameter	2 populations: - $d_{p,1}$ = 33 µm - $d_{p,2}$ = 183µm (3 samples)	

2.2 Experimental bench

The bench used for velocity and pressure drop measurements is shown in Fig. 1. It consists mainly of a straight stainless-steel duct of 150 x 150 mm² cross-section and 3 m in length. The measurement zone, where the filter is located, is made of transparent antistatic PMMA to enable viewing and control of the velocity sensor position in relation to the filter. The filter is located at a distance of x = 167 cm from the duct entrance. High-efficiency filters H14 (EN 779:2012) are located at the entrance and exit of the duct to ensure clean air conditions inside it. The pressure drop generated by the filter is measured with a differential pressure sensor. It was measured for a mean duct velocity ranging from 0 to 1.56 $m.s^{-1}$, which corresponds to a hydraulic Reynolds number range of 0 - 15,750 and a filtration velocity range of 0 - 0.65 $m.s^{-1}$. The mean duct velocity V_{mean} and the filtration velocity $V_{filtration}$ are calculated as follows:

$$V_{mean} = \frac{Q_{bench}}{S_{bench}} \quad (1)$$

$$V_{filtration} = \frac{Q_{bench}}{S_{filtration}} \quad (2)$$

Where Q_{bench} is the volumetric air flow rate in the bench, S_{bench} is the duct surface and $S_{filtration}$ is the developed medium surface.

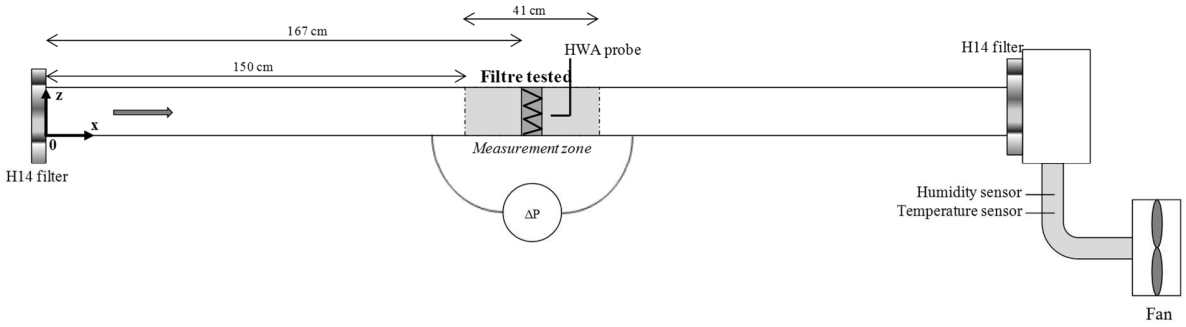

Fig. 1. Diagram of experimental bench (for velocity measurements downstream of the filter).

2.3 Velocity measurements

Velocity measurements were carried out upstream and downstream of the filter by Hot Wire Anemometry (HWA) using a Dantec© Constant Temperature acquisition chain. This technique, used for local velocity measurements, was selected because it allows high-frequency acquisitions and does not require the use of particulate tracers like laser techniques. These measurements were carried out at the nominal filtration velocity of the fibrous medium recommended by the supplier, i.e. $V_{filtration}$ = 0.27 $m.s^{-1}$. The mean duct velocity required to achieve this value is V_{mean} = 0.67 $m.s^{-1}$, and the corresponding hydraulic Reynolds number is 6,760, hence the flow regime in the duct is transitional.

The airflow characterization consisted of acquisition of transversal velocity profiles (i.e. through the y-axis) (see Fig. 2), at different x positions upstream and downstream of the filter. The displacement system used to control the position of the probe was made of two perpendicular calipers allowing displacements in directions x and y (see Fig. 2 (a)) with 10 µm precision.

Before measuring the airflow in the vicinity of the filter, a set of experiments was performed without the filter to characterize the airflow in the measurement zone, at the mean duct velocity previously mentioned (V_{mean} = 0.67 m.s^{-1}). For this purpose, a straight probe (55P11, Dantec ©) mounted on a straight support was used. The probe calibration involved 30 points between 0.10 and 1.60 m.s^{-1}. Transversal velocity profiles were recorded at three z positions (at the duct center, i.e. z = 7.5 cm, at z = 9.5 cm and at z = 5.5 cm). This enabled determination of the boundary layer thickness of the vertical and horizontal duct walls and the mean velocity at the duct center. For the mean duct velocity tested (V_{mean} = 0.67 m.s^{-1}), the boundary layer thickness was δ = 45 mm and the mean velocity at the duct center was V_{center} = 0.80 m.s^{-1}.

The displacements through the y axis corresponding to the velocity measurements downstream of the filter are presented in Fig. 2 (b). For these measurements, a straight probe (55P11, Dantec ©) mounted on a straight support was used. The calibration of the anemometry probe involved 45 points between 0.1 and 3.0 m.s^{-1}. For each measurement point, the frequency and the sampling time were 200 Hz and 60 s respectively. For each prototype, these transverse velocity profiles were recorded downstream of the four half-pleats located in the bulk flow, i.e. outside the boundary layer, as shown in Fig.2 (a). Since these measurements were carried out for the three filter prototypes, a total of twelve half-pleats were characterized. For each half-pleat, transversal velocity profiles were acquired at five x distances downstream of the pleat peak (for this point we considered a longitudinal coordinate x = 0 cm), as shown in Fig.2 (b): x = 1.5; 2.0; 3.0; 3.5 and 5.0 cm. These measurements were taken at the height z = 7.5 cm, i.e. half the height of the duct. The y step of the probe displacements was 1 mm. For the two profiles acquired inside the pleat (x = 1.5 and 2.0 cm), the minimum distance to the medium surface at which the measurements were carried out was 1 mm.
Transverse velocity profiles were also acquired upstream of the filter as shown in Fig.2 (c). These measurements were carried out inside one half-pleat (x = 0.2 cm; 1.0 and 1.3 cm) with a right-angled hot wire probe (55P13, Dantec©) mounted on a straight support. The probe was inserted inside the pleat through a hole drilled on the filter prototype frame. For each measurement point the frequency and sampling time were 200 Hz and 60 s respectively. The calibration of the anemometry probe involved 45 points between 0.1 and 3.0 m.s^{-1}. The y step of the probe displacements was 1 mm. The minimum distance to the medium surface at which these measurements were carried out was 5 mm.

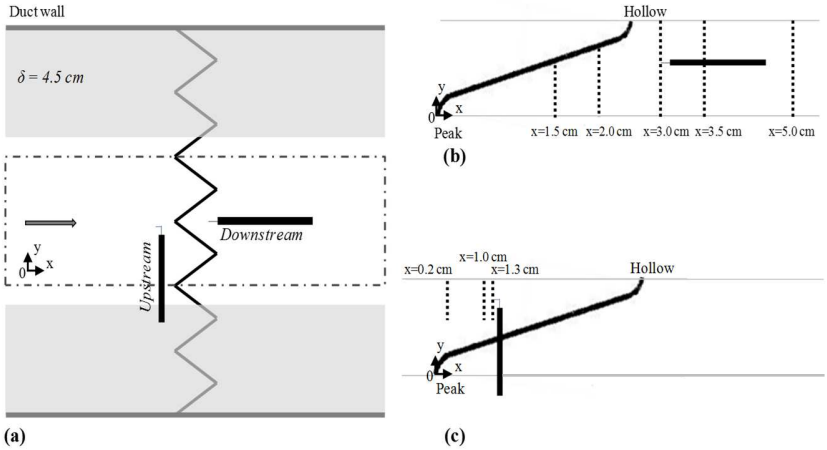

Fig. 2. Diagram of hot wire probe displacements: (a) top view of filter; (b) transverse displacements downstream of one half-pleat; (c) transverse displacements upstream of a one half-pleat.

2.4 Numerical simulations

2.4.1. Computational domain and boundary conditions

Numerical simulations were carried out with the commercial code ANSYS Fluent©. A numerical domain consisting of a two-dimensional mesh was generated to simulate the flow through one half-pleat. It was divided into two domains: a fluid representing air and its thermodynamical characteristics at 20°C, and a porous material representing the fibrous medium. The half-pleat was positioned after a straight length of 251 mm, within a total length of 550 mm, corresponding to the real distance between pressure samplers located upstream and downstream of the filter used to calculate the pressure drop.

A mesh convergence study was carried out to determine the optimal mesh sizes to ensure an independent solution. A non-structured meshing, refined in the air layer (of 0.3 mm thickness) close to the media surface, was adopted. The mesh size in this zone was 0.1 mm. It was checked that a more refined mesh does not modify the pressure drop and the velocity profiles. For the rest of the domain a mesh size of 0.2 mm was adopted. The mesh convergence stabilized for around 210,000 mesh elements.

The boundary conditions used are presented in Fig. 3. The half-pleat was inserted between two symmetry conditions. A constant velocity inlet value was placed at the domain inlet. At the domain outlet a pressure outlet of 101,325 Pa was fixed.

The shaded areas in Fig. 3 correspond to the porous medium. The manufacturing process of the pleated filter may have produced local modifications in the structural properties of the curved zones of the fibrous medium (represented in grey in Fig. 3). Since these modifications are difficult to measure, especially those affecting the thickness and permeability of the medium, it was assumed that the local permeability in this zone ranged between a low value, relating to the extreme case of non-permeability, and the same permeability as elsewhere along the pleat. To evaluate the sensitivity of the pressure drop to the local permeability of the pleat curved zones, as suggested by Rebaï et al. [4], two simulation series were carried out, considering the zones as permeable or non-permeable.

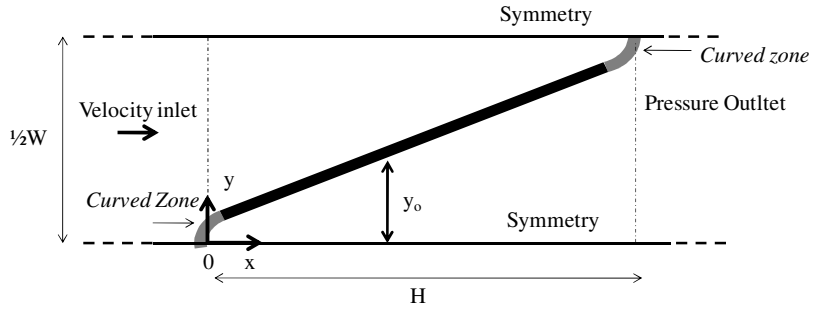

Fig. 3. Simulation domain and boundary conditions.

2.4.2. CFD models and equations

The airflow was modeled by the Navier-Stokes equations at steady state. The range of inlet air velocity (or mean duct velocity for the purpose of experiments) for which the numerical and experimental pressure drop were compared was 0 - 1.56 $m.s^{-1}$. The corresponding hydraulic Reynolds number range on the bench was Re_h = 0 - 15,750. This range of airflow conditions therefore covers laminar and turbulent flow regimes, including transitional flow regimes. This is why three models; the laminar model, the standard k-ε turbulence model and the transition SST model, were tested to assess their ability to predict the filter pressure drop and local velocity patterns for the inlet velocity value of 0.67 $m.s^{-1}$ (Re_h = 6,760). The standard k-ε turbulence model is widely used to solve the NS equations, using two equations (turbulent kinetic energy k and its dissipation rate ε). This model better suits free shear flows (away from walls) with low pressure gradients. According to the literature, this model succeeds in predicting the pressure drop for unused pleated filters with low permeability [11,18]. The transition SST model consists of coupling the k-ω SST transport equations (combination of the k-ω model used in near-wall areas and the k-ε model applied in internal shears areas) with two other transport equations: one for transition onset criteria and one for intermittency, regarding momentum-thickness Reynolds number. According to the literature, none of the studies dealing with numerical simulations of airflow in the vicinity of pleated filters [4,5,11-17] concerned the transient flow regime. Regarding the Reynolds number range mentioned above, therefore, it is useful to test the ability of a transition model such as the transition SST to predict the pressure drop and airflow in the vicinity of pleated filters.

For the filtration velocity range for which the pressure drop was measured (0 - 0.65 $m.s^{-1}$), the pore Reynolds number Re_p was calculated using the following equation:

$$Re_p = \frac{\rho V_{filtration} d_p}{\mu} \quad (3)$$

Where μ and ρ are the air dynamic viscosity and density, $V_{filtration}$ is the filtration velocity and d_p is the modal pore diameter of the fibrous medium.

According to the literature, the inertial regime initiates at a Re_p between 1 and 10 and persists at a $Re_p \sim 150$ [22]. Deviation from the linearity is relatively weak for $1 \leq Re_p \leq 3$.

The fibrous media of which the studied filter is made presents two pores populations, characterized by modal diameters d_{p1} = 33 µm and d_{p2} = 183 µm (see Table 1). For the velocity range tested for pressure drop characterization, and by considering d_{p1} in the calculations (which is the most important population), Re_{p1} = 0 - 1.44. For the largest pore diameter d_{p2} =183 µm (which is the less important population), Re_{p2} = 0 - 8.01. This means that the initiation of the

inertial regime is reached for the maximum velocity tested. The inertial resistance to the flow of the medium is therefore assumed to be negligible and the pressure drop that it generates is predicted using the Darcy equation:

$$\Delta P = \frac{\mu z}{\beta} V_{filtration} \quad (4)$$

Where z is the thickness of the medium and β its permeability. The medium is assumed to be isotropic.

3. Results and discussion

3.1 Prediction of filter pressure drop

3.1.1. Influence of airflow model on pressure drop

Fig. 4 compares the experimental and numerical filter pressure drop for the filtration velocity range 0 - 0.65 $m.s^{-1}$. The experimental data are the mean pressure drop obtained from the measurements carried out on the three prototypes, and the vertical error bars represent the minimum and maximum values. The mean filtration velocities and their horizontal error bars correspond to the average, minimum and maximum filtration velocity values calculated from the developed surface areas of the three filter prototypes. These surfaces are not exactly the same due to the lab-scale manufacturing process for the prototypes. For the filtration velocity range in question, the pressure drop values obtained by CFD calculations are not significantly influenced by the airflow model (laminar, standard k-ε and transition SST). The maximum deviation between two pressure drop values obtained with two models is 2% (223 Pa compared to 220 Pa for the laminar model and k-ε model respectively at a filtration velocity of 1.56 $m.s^{-1}$). Therefore, to analyze the sensitivity of the numerical pressure drop to the geometrical properties of the pleat and the permeability of its curved zone, presented in Fig. 4, the numerical pressure-drop results shown are those obtained with the laminar model.

The fact that the pressure drop is not influenced by the airflow model has already been reported in the literature. For example, Feng et al. [18] showed that the large eddy simulation, the detached eddy simulation, the low Re k-ε, the standard k-ε and the v2f models can predict the pressure drop at low filtration velocity ($V_{filtration}$ = 0.072 $m.s^{-1}$) for rectangular pleats (H = 50 mm, W = 50 mm) and low-permeability media (β = $8.33.10^{-12}$ m^2). Theron et al. [11] showed that the Reynolds stress and standard k-ε models give similar pressure drop to that measured experimentally for the filtration velocity range 0.14 - 0.79 $m.s^{-1}$ with a filter with triangular pleats (H = 40 mm, W = 23 mm) and medium permeability of $2.0.10^{-9}$ m^2. On the other hand, Rebaï et al. [4] tested the same turbulence models as Feng et al. [18] and did not obtain a similar pressure drop for triangular pleats (H = 51 mm, W = 12.5 mm) and medium permeability of 3.57. 10^{-10} m^2, for $V_{filtration}$ = 0.39 $m.s^{-1}$. Tronville et Sala [17] showed that for the inlet velocity range 0.2 - 1.0 $m.s^{-1}$, the Reynolds stress model (RSM) was the best of three models (RSM, standard k-ε and RNG k-ε) for predicting the pressure drop of a mini-pleated filter (H = 25 mm, W = 3.2 mm) and a low permeability medium (β = $7.5.10^{-12}$ m^2). In conclusion, it is not possible to give general recommendations for selecting a relevant airflow model, even to predict the pressure drop, as it depends on the airflow conditions and the properties of the filter and medium.

3.1.2. Influence of pleat geometry and curved pleat zone permeability on pressure drop

The results presented in Fig. 4 show that the CFD calculations reproduce the order of magnitude of the experimental pressure drop quite well, even if they tend to under-predict it, especially as the filtration velocity increases. The numerical pressure drop reported in Fig. 4 have been obtained using the Darcy's equation. Simulations with the Darcy-Forchheimer equation, i.e. by taking into account the inertial resistance of the fibrous medium to the airflow, have been also done. But for the considered filtration velocity range (0 - 0.65 $m.s^{-1}$), a negligible influence on the pressure drop was obtained.

The sensitivity of the numerical pressure drop to two parameters was evaluated in an attempt to explain this deviation. Fig. 4 (a) depicts the sensitivity of the numerical pressure drop to the geometric properties of the pleat. The pleats of the prototype filter may in fact vary in height and width due to laboratory manufacturing. Their heights and widths were 28 ± 1 mm and 25 ± 1 mm respectively. The pressure drop values in Fig. 4 (a) represent the mean height and width (H = 28 mm, W = 25 mm) and the value obtained with the sets of parameters representing the maximum (H = 29 mm, W = 24 mm) and minimum (H = 27 mm, W = 26 mm) pressure drop.

Fig. 4 (a) shows that the pressure drop is very sensitive to pleat geometric properties. This aspect has also been pointed out by Theron et al. [11]. The pressure drop increases with lower pleat width and higher pleat height, which concurs largely with tendencies reported in the literature for different filter properties and flow conditions [4,11,12,14]. Consequently, the maximum deviation between experimental and numerical pressure drop for the filtration velocity range studied is reduced from 20% with mean pleat height and width (H = 28 mm, W = 25 mm) to 15% with the set of parameters H = 29 mm and W = 24 mm.

Fig. 4 (b) represents the sensitivity of the numerical pressure drop to the pleat curved zone permeability. The results show that the simulated pressure drop (calculated with mean pleat width and height) increases when the pleat curved zones are considered impermeable. The deviation between numerical and experimental pressure drop is reduced to 16%. With the set of parameters H = 29 mm and W = 24 mm; the deviation between numerical and experimental pressure drop was reduced to 12%. These results are in accordance with the CFD simulation results of Rebaï et al. [4]. This can be explained by the fact that the total available filtration area is reduced, causing the pressure drop to increase. The air streamlines approaching the impermeable curved zone are deviated, which leads to increased air drag due to the higher velocity in the pleat channel and consequently to increased pressure drop across the filter.

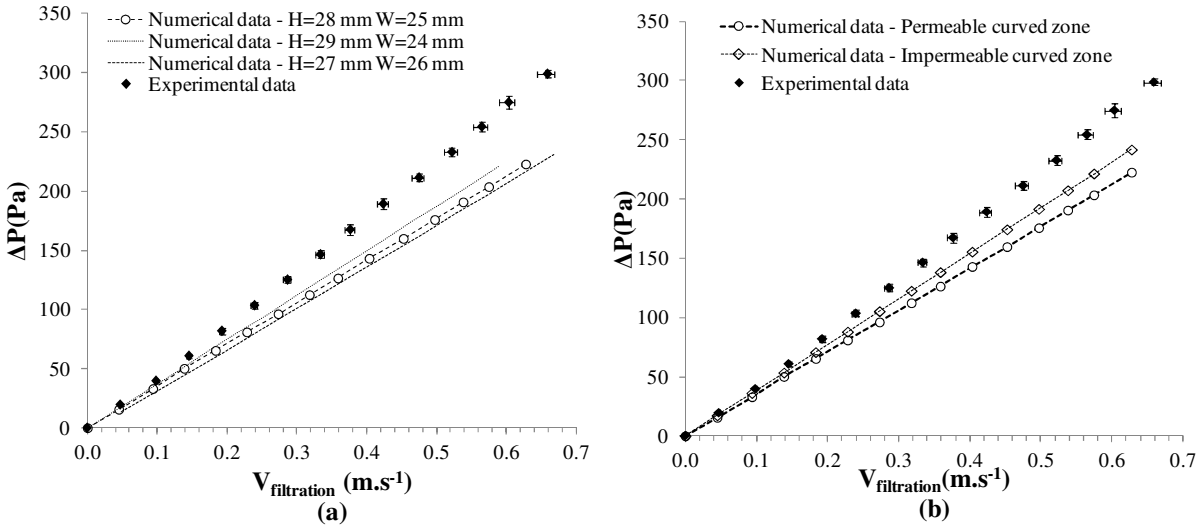

Fig. 4. Comparison of experimental and numerical filter pressure drop: sensitivity analysis of (a) pleat geometric properties (b) pleat curved zone permeability (with H = 28 mm and W = 25 mm).

To summarize, the simulated pressure drop obtained with the highest pleat height and lowest pleat width (H = 29 mm, W = 24 mm) is closest to the experimental pressure drop for the permeable curved zone. In addition, the pressure drop gets closer to the experimental values when the curved zone is considered impermeable. The airflow model has no effect on the pressure drop, irrespective of whether the laminar, standard k-ε or transition SST model is used. The experimental pressure drop at the filtration velocity tested in this study ΔP_{exp} ($V_{filtration}$ =0.27 m.s^{-1}) = 117 Pa is close to the value found numerically with the laminar model ΔP_{num} ($V_{filtration}$ = 0.27 m.s^{-1}) = 108 Pa ($Error_{exp\text{-}num}$ ~ 8%). Since the pressure drop is a macroscopic parameter, it is useful to analyze the respective ability of these models to predict local values like velocity, especially in the vicinity of the filter where significant velocity gradients are expected. In comparing experimental and numerical velocity data, the mean pleat height and width (H = 28 mm and W = 25 mm) are used, as these are considered representative of the actual geometric parameters of the prototypes pleats.

3.2 Velocity patterns

3.2.1 Numerical velocity fields in the vicinity of the filter

Fig.5. shows the velocity field in the vicinity of the half-pleat obtained by CFD for the three airflow models tested (laminar, standard k-ε and transition SST) for V_{mean} = 0.67 m.s^{-1} (corresponding to $V_{filtration}$ = 0.27 m.s^{-1}). These three velocity fields show that no significant velocity gradients are detected upstream of the pleat for this filtration velocity, while significant gradients are observed downstream of the pleat whatever the airflow model. Upstream of the filter the velocity tends to be homogeneous and close to the mean duct velocity (0.67 m.s^{-1}) approaching the filter. Downstream of the filter velocity values of up to 1.7 m.s^{-1}, i.e. 2.5 times higher than the mean duct velocity, are achieved. These velocity patterns also show that local velocity values downstream of the filter are greatly influenced by the airflow model. The subject of the next section is therefore a comparison between experimental and numerical velocity profiles downstream of the filter.

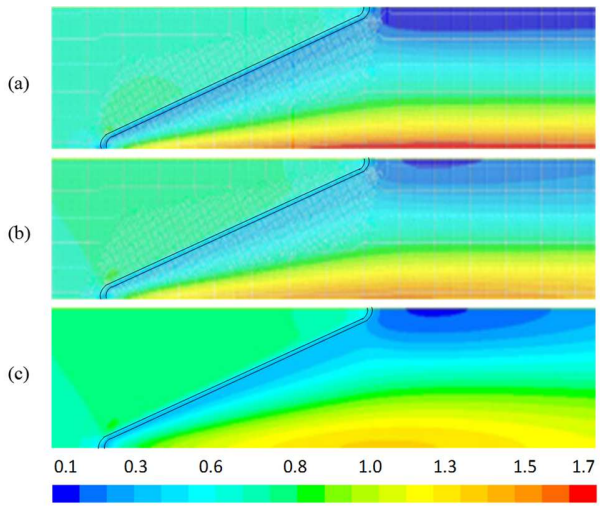

Fig. 5. Numerical velocity fields obtained for three airflow models: (a) laminar, (b) transition SST, (c) standard k-ε.

3.2.2 Experimental velocity profiles downstream of the filter

Two representations are given of the experimental transversal velocity profiles downstream of the filter (see Fig. 7). The data in Fig. 7 (a) represent the evolution of the velocity along the y coordinate for different longitudinal x positions. In this graph, y = 0 cm represents the bottom symmetry line, i.e. the symmetry axis passing through the pleat peak, as depicted in Fig. 6. In Fig. 7 (b) these profiles are presented as dimensionless values: the velocity is normalized by the mean duct velocity (V_{mean} = 0.67 m.s^{-1}) and the vertical coordinate y is normalized by y_0, defined as the distance between the symmetry axis passing through the pleat peak and the medium surface at the x coordinate in question. The ratio y/y_0 is thus equal to 0 at the bottom symmetry line, and to 1 at the medium surface, as illustrated in Fig. 6.

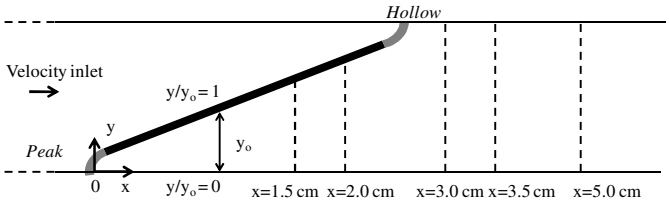

Fig. 6. Diagram of the dimensionless coordinate y/y_0 adopted to represent the transversal velocity profiles downstream of the filter.

The experimental velocity data presented in Fig. 7 consists of the average values of the recordings made for the four central half-pleats of the three prototypes (twelve half-pleats in total). The error bars in Fig. 7 (a) represent the corresponding standard deviations. All the measurement points presented in Fig. 7 (a) reveal fairly small error bars, confirming that the results are highly reproducible and that the Hot Wire Anemometry technique is appropriate for these measurements, even inside the pleats and in close proximity to the filter medium (1 mm). The most significant deviations are recorded downstream of the pleat peak (i.e. for y values of 0 to 2 mm). This can be explained by the fact that this zone is located directly downstream of a curved portion of the pleat that might exhibit local deviations of the structural properties of the medium (porosity, thickness, permeability, etc.), and/or deviations in the shape of the curved

zones due to the manual pleating process. These velocity deviations are less pronounced downstream of the pleat hollow. This may be because the measurement points in this zone are very close to the medium and the air velocity is therefore lower than elsewhere in the pleat channel. Some small irregularities in terms of pleat height and width can also lead to non-negligible deviations of the velocity profiles, which may also explain the general amplitude of the error bars.

Fig. 7 (a) shows that all the velocity profiles are similar in shape. The velocity reaches a maximum at y = 0 mm; at this point the ratio V/V_{mean} is close to 3 whatever the x coordinate concerned, as observed in Fig. 7 (b). The velocity then decreases as y increases. For the two profiles inside the pleat (x = 1.5 and 2.0 cm), the minimum recorded velocity V_{min}, i.e. in closest proximity to the medium surface, is near to the filtration velocity of 0.27 $m.s^{-1}$ (see Table 5). For the three velocity profiles outside the pleat (x = 3 - 5 cm), the minimum velocity recorded is 0.14 $m.s^{-1}$. This velocity is detected downstream of the pleat hollow where low velocity variations are observed (see Fig.5). As mentioned previously, this can be explained by the fact that this zone of the filter is located directly downstream of a curved pleat zone. In addition, Fig. 7 (a) shows that at the three positions outside the filter (x = 3 - 5 cm) the profiles are identical. It therefore reveals that the geometric properties of the filter and airflow conditions concerned lead to significant velocity gradients downstream of the filter and persist for at least 2.5 cm downstream of the filter (2.5 cm in height). Fig. 7 (a) also shows that the velocity profiles are sharper going deeper into the pleat (i.e. x decreases). This is basically due to the continuous reduction of available space for flow along the pleat length in the case of triangular pleats.
When the velocity profiles are presented as dimensionless parameters they are identical, as observed in Fig. 7 (b). A similar result was obtained by Rebaï et al. [4]: the normalized velocity profiles (using dimensionless parameters similar to those previously described) obtained numerically at eight positions inside the pleat channel (x = 0.5 - 4.5 cm) were fairly similar for the filtration velocity $V_{filtration} = 0.39$ $m.s^{-1}$.

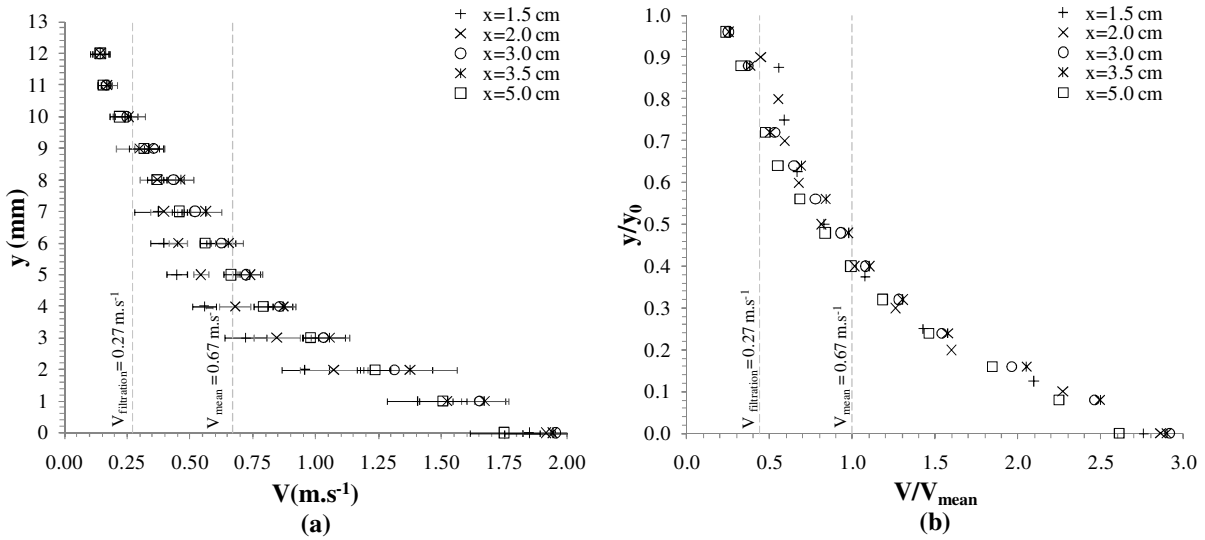

Fig. 7. Experimental transversal velocity profiles downstream of the filter for $V_{mean} = 0.67$ $m.s^{-1}$ ($V_{filtration} = 0.27$ $m.s^{-1}$).

3.2.3 Numerical versus experimental velocity profiles downstream of the filter

Fig. 8. compares experimental and numerical velocity profiles obtained with the three airflow models downstream of the filter, at two x positions: x = 2.0 cm, i.e. inside the pleat, and x = 3.5 cm i.e. outside the pleat (Fig. 6). The three numerical profiles agree quite closely with the experimental one for $y \geq 2$ mm. For this y coordinate range, the data obtained with the laminar and transition SST models, in particular, are identical and almost all appear inside the error bars of the experimental values. For $y \leq 2$ mm, the discrepancies between the numerical velocity values are more significant. This can be explained by the fact that this zone is located downstream of a curved zone of the pleat (the pleat peak) which gives rise to high-velocity gradients difficult to capture numerically. Also, as mentioned previously (see sections 3.1 and 3.2.2), in this zone the filter medium may be subject to modifications of its structural properties (porosity, thickness, permeability) which are difficult to reproduce numerically and may influence airflow behavior. These observations concur closely with the numerical results produced by Rebaï et al. [4], who showed that the structural properties of the medium in the pleat curved zones are modified by the pleating process and that resistance to flow increases in this area, which may affect the airflow pattern locally. Similar deviations have also been reported by Kang et al. [15], who compared their experimental velocity profiles obtained by Particle Image Velocimetry (PIV) downstream of a custom-built rectangular pleated filter (H = 50.4 mm, W = 50.4 mm) with numerical values obtained by CFD. They showed that the DES model proposed by Feng et al. [18] succeeded in reproducing the experimental results except in close proximity to the pleat curved zone. Similar curve shapes were obtained for the other x coordinates downstream of the filter (x = 1.5, 3.0 and 5.0 cm), whether located inside or outside the filter, and the same conclusions can be drawn.

To summarize, the overall trends for velocity profiles obtained using HWA and CFD calculations concurred closely for the three numerical airflow models tested, except near the pleat curved zone. The laminar model was revealed as the one best able to reproduce the velocity distribution downstream of these zones. The next section addresses the issue of sensitivity of velocity profiles downstream of the filter to the permeability of pleat curved zones. In respect of the considerations mentioned above, only data obtained with the laminar model will be given for the analysis of numerical velocity profiles.

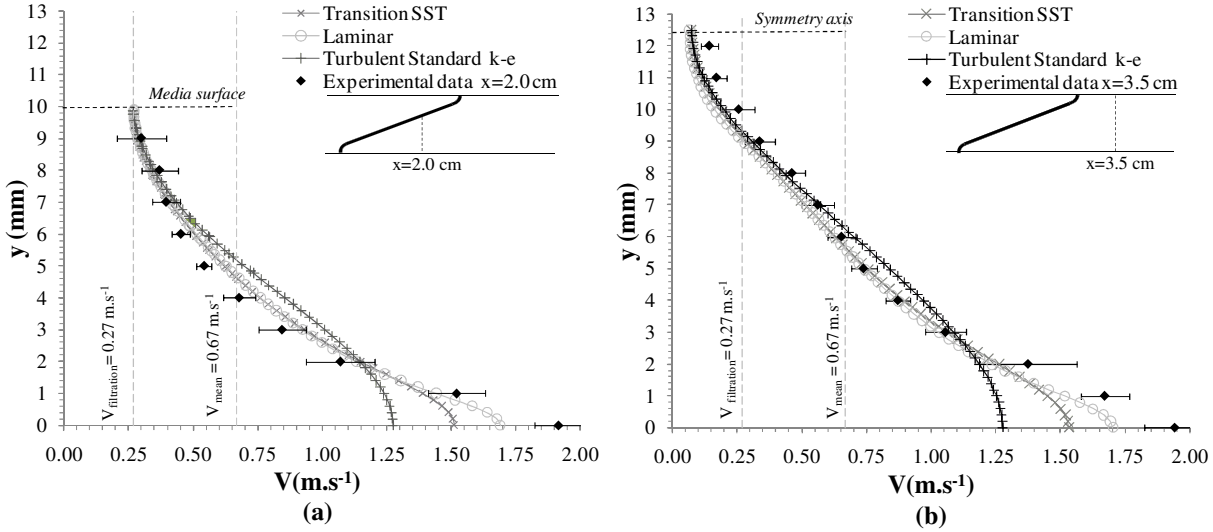

Fig. 8. Comparison of numerical and experimental transversal velocity profiles downstream of the filter for V_{mean} = 0.67 m.s^{-1} ($V_{filtration}$ = 0.27 m.s^{-1}): at (a) x = 2.0 cm; and at (b) x = 3.5 cm.

3.2.4 Influence of pleat curve- zone permeability on numerical velocity profiles downstream of the filter

As mentioned previously (see section 3.1), considering the pleat curved zone as impermeable significantly influences the pressure drop. The effect of such an assumption on the velocity distribution downstream of the filter is addressed in this section. Fig. 9 compares the numerical velocity profiles (calculated with the laminar airflow model) for permeable and impermeable curved zones of the pleat at two x coordinates downstream of the filter: x = 2.0 cm (i.e. inside the pleat, Fig. 9 (a)), and x = 3.5 cm (i.e. outside the pleat, Fig. 9 (b)). At x = 2.0 cm, the numerical velocity profiles are perfectly identical, except for y ≤ 1 mm, i.e. downstream of the pleat peak, where the velocity for the impermeable pleat peak slightly decreases by 4% compared to that for the permeable one. Similar results were obtained for the other x coordinate located inside the pleat (x = 1.5 cm). At x = 3.5 cm (Fig. 9 (b)), the numerical velocity profile obtained with impermeable curved zones is identical to that with completely permeable ones, except for y ≥ 9 mm. From this position the velocity starts to decrease and reaches a null value at y = 10.5 mm, i.e. downstream of the pleat hollow. It then increases to become identical with the numerical value obtained for the completely permeable ones and the experimental value at the end of the curve. Similar curve shapes were obtained for all x coordinates studied downstream, outside of the filter (x = 2.0 and 5.0 cm). These results show that assuming the curved pleat zones to be non-permeable has a significant effect on velocity distribution downstream of this zone outside the pleat, more precisely downstream of the pleat hollow, but becomes less pronounced elsewhere along y, or inside the pleat.

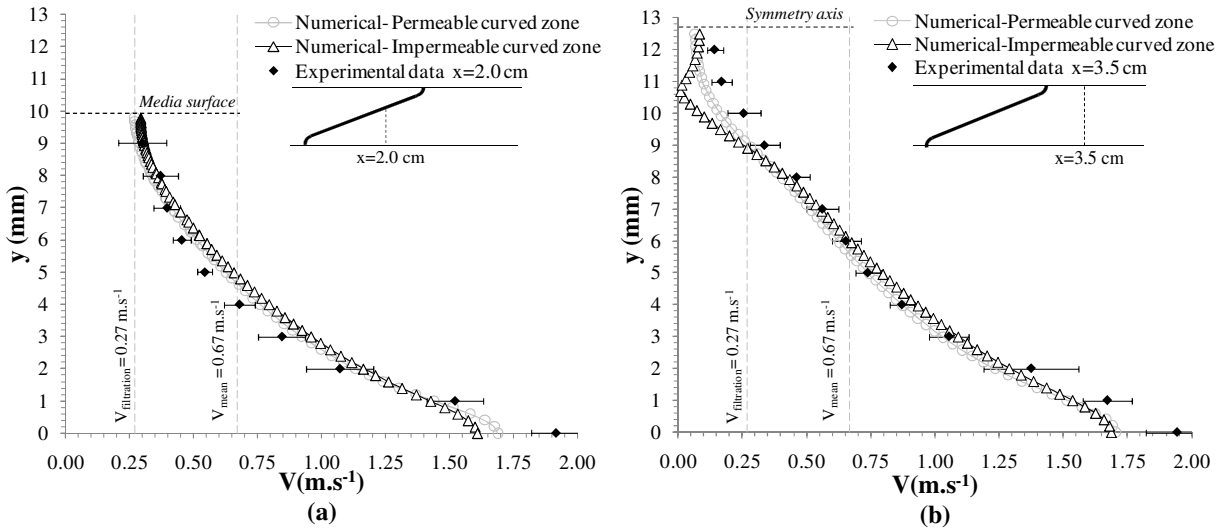

Fig. 9. Influence of pleat curved-zone permeability on numerical velocity profiles (calculated with the laminar airflow model) downstream of the filter for V_{mean} = 0.67 m.s^{-1} ($V_{filtration}$ = 0.27 m.s^{-1}): at (a) x = 2.0 cm; and at (b) x = 3.5 cm.

3.2.5 Numerical versus experimental velocity profiles upstream of the filter

Fig. 10 (a) compares the experimental velocity profiles upstream of the filter at three x coordinates x = 0.2 cm, x = 1.0 cm and x = 1.3 cm (the coordinate x = 0 cm corresponds to the pleat peak, as shown in Fig.10) to those obtained numerically using the laminar airflow model. The experimental velocity profiles involve y coordinate ranges mostly located in the center of the pleat. The minimum distance from the filter medium at which the velocity was recorded was 2.0 mm for the profile at x = 1.3 cm. Fig. 10 shows that the numerical velocity values in this pleat zone are equal to the experimental ones, confirming that the laminar flow model is relevant for predicting the velocity pattern for the airflow conditions tested.

In addition, these experimental and numerical profiles show that despite the mean airflow approaching the filter being fairly transitional (Re_h = 6,760) at the pleat center, the velocity is homogeneous and almost equal to the mean duct velocity (V_{mean} = 0.67 m.s^{-1}). The numerical simulations that produce velocity data up to the medium surface indicate that velocity decreases sharply within a very thin air film, approximately 0.3 mm thick, at the medium surface, with values in the order of $V_{filtration}$ (0.27 m.s^{-1}). For the airflow in question, this result supports the decision to use the laminar flow model. More generally it raises the issue of the relevant Reynolds number to be considered when selecting the appropriate airflow model for air velocity patterns inside the filter pleats. According to Rebaï et al. [4], the flow inside the pleat channel can be characterized by the channel Reynolds number, which takes into account the mean duct velocity and half-pleat width as the characteristic length:

$$Re_w = \frac{\rho V_{mean} 0.5W}{\mu} \quad (5)$$

For the present case, Re_w is equal to 560, which is quite low and may justify the choice of the laminar airflow model. For some cases reported in the literature, significant velocity gradients were detected upstream of the pleat, with maximum velocity values in the central pleat zone considerably higher than the mean duct velocity approaching the filter. These studies, however, are characterized by a turbulent airflow regime approaching the filter. For example, the CFD simulation of Theron et al. [11] showed that for V_{mean} =2.8 m.s^{-1}, corresponding to Re_h = 22,480 and Re_w = 2150 and 1080 (for W = 23 and 11.5 mm respectively), the velocity was over 5 times the mean duct velocity at the pleat center upstream of the filter. These considerations might indicate that in terms of the airflow inside the pleat, the onset of turbulence appears at a channel Reynolds number between 560 and 1080. However, the numerical simulation of Rebaï et al. [4] for $V_{filtration}$ = 0.39 m.s^{-1} and Re_w = 1097 (for W = 4 mm) showed that the velocity varied slightly at the pleat center upstream of the mini-pleated filter and barely reached 1.1 times the mean duct velocity, which is close to the results obtained in the present study. The appearance of turbulence on the upstream side of the pleat therefore depends on a number of parameters (filtration velocity, filter geometry and structural properties), and further assessment is required to determine the transition channel Reynolds number above which the turbulence starts to occur.

The numerical velocity profiles in Fig.10 (b) enable evaluation of the scale of local velocities at which particles might reach the filter at the air/filter interface (0 mm from the medium surface) and two distances from the medium surface: 0.05 and 0.10 mm. For the straight part of the pleat located at 0.10 mm above the surface of the medium, i.e. for x coordinates between 1 and 27 mm, the velocity ranges between 0.74 m.s^{-1} and 0.44 m.s^{-1}, which represents 2.7 to 1.6 times the theoretical filtration velocity ($V_{filtration}$ = 0.27 m.s^{-1}). The scale of local velocity variation decreases considerably approaching the surface of the medium. The velocity ranges between 0.60 m.s^{-1} and 0.41 m.s^{-1} along the straight line 0.05 mm above the surface of the medium, and between 0.46 m.s^{-1} and 0.35 m.s^{-1} along the straight line on the surface, which represents 2.2 - 1.5

and 1.7 - 1.3 times the theoretical filtration velocity respectively. These results show that even though the airflow upstream of the pleat is mostly laminar, some velocity gradients may appear close to the surface of the medium. They are less significant, but they may generate some local particle collection efficiency gradients.

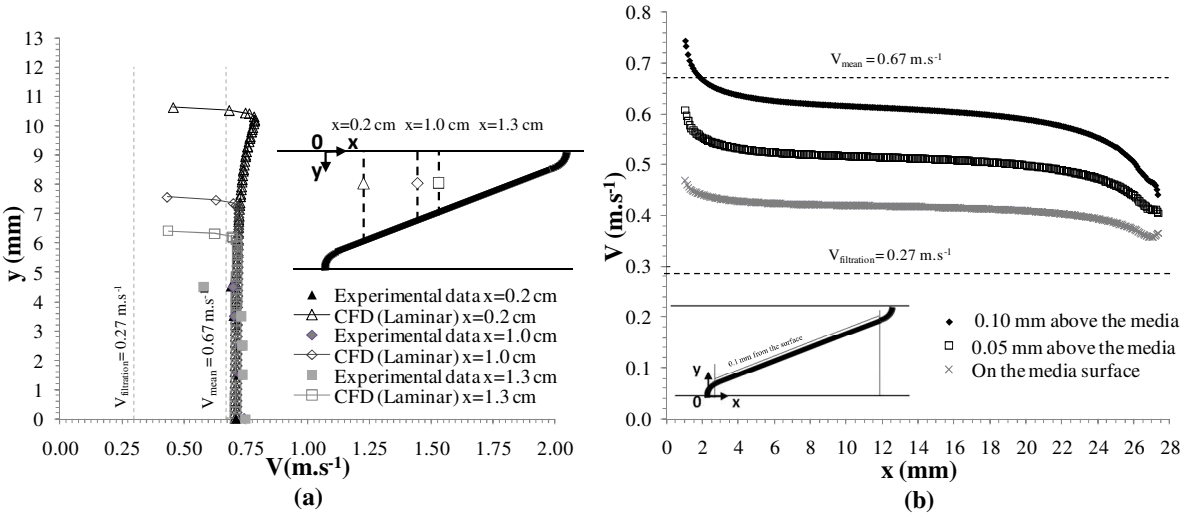

Fig. 10. (a) Numerical (calculated with the laminar airflow model) and experimental transversal velocity profiles upstream of the filter at x = 0.2 cm, x = 1.0 cm and x = 1.3 cm for V_{mean} = 0.67 m.s^{-1} ($V_{filtration}$ = 0.27 m.s^{-1}). (b) Numerical longitudinal velocity profiles at the air/filter interface and at 0.05 mm and 0.10 mm from the medium surface.

3.3 Turbulence intensity profiles

Of the few studies in the literature that have reported experimental velocity recordings in the vicinity of the filter [14,15,18], none has shown turbulence intensity values, to our knowledge. The turbulence intensity TI represents the ratio of the root-mean-square fluctuating velocity v'_{rms} to the average velocity $\overline{V}$:

$$TI = \frac{v'_{rms}}{\overline{V}} \quad (6)$$

For the mean duct velocity in question of 0.67 m.s^{-1}, the velocity recordings made in the empty duct led to mean TI values at the duct center of 7%. Fig. 11 (a) shows TI profiles upstream of the pleat at the x positions considered in the previous section. Each point corresponds to one measurement taken in a single half-pleat. The turbulence intensity varies slightly along y for the three profiles, ranging from 6% to 7% at x = 0.2 cm, and from 5% to 6% at x = 1.0 cm and 1.3 cm. These results show that velocity fluctuations seem to decrease going deeper inside the pleat.

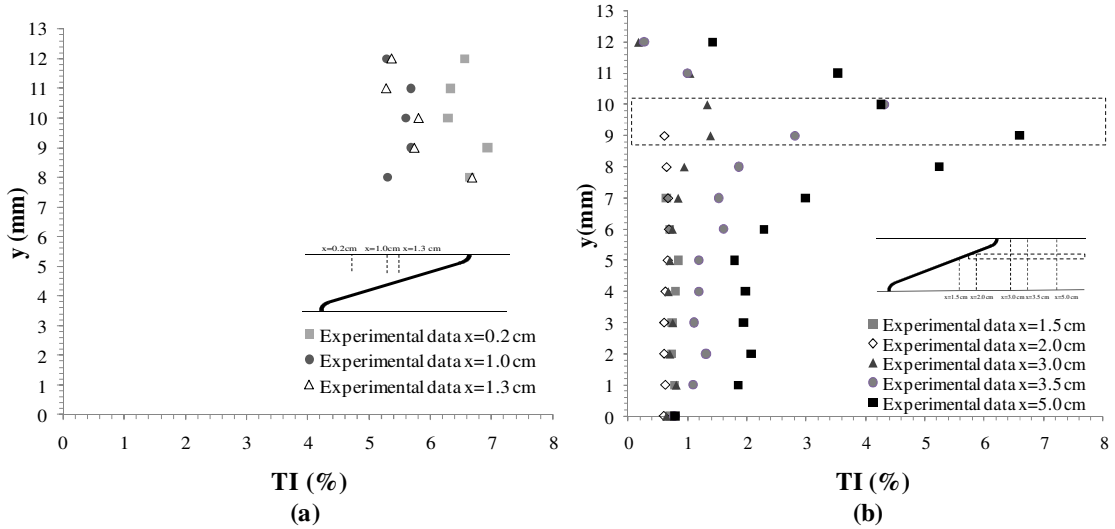

Fig. 11. Experimental transversal turbulence intensity profiles for V_{mean} = 0.67 m.s^{-1} ($V_{filtration}$ = 0.27 m.s^{-1}) (a) upstream of the filter at x = 0.2 cm, x = 1.0 cm and x = 1.3 cm; (b) downstream of the filter at x = 1.5 cm, x = 2.0 cm, x = 3.0 cm, x = 3.5 cm and x = 5.0 cm.

Fig. 11 (b) shows the experimental turbulence intensity profiles at each x position discussed previously, downstream of the filter (see sections 3.2.2 to 3.2.4). Like for the velocity profiles, the TI values represent average values for the twelve half pleats. Turbulence intensity at the x positions inside the pleat is almost constant and very low: it varies slightly, around 0.8% at x = 1.5 cm and around 0.6% at x = 2.0 cm. This result indicates that the airflow turbulence level decays by passing through the fibrous medium, and confirms that the flow regime inside the pleat is fairly laminar. The turbulence intensity increases outside the pleat as the distance from the filter x increases. The maximum values detected were all lower than 7%, which corresponds to the turbulence intensity value of the empty duct. The TI profiles measured at x = 3.0, 3.5, and 5.0 cm produce similar shapes: the TI is almost constant downstream of the straight part of the pleat, and increases downstream of the pleat hollow to reach a peak at y = 9 mm downstream of the curved part of the filter. This increase may be due to the complex shape of the pleat and the locally-modified structural properties of the medium.

To summarize, the turbulence intensity profiles downstream of the filter showed a very low gradient inside the pleat and an increase outside the pleat, especially downstream of the pleat hollow. At the filtration velocity tested ($V_{filtration}$ = 0.27 m.s^{-1}), no significant turbulence intensities were detected close to the medium surface. However, it would be useful to measure turbulence intensities for higher mean duct velocity values, especially downstream of the filter, since as reported by Maddineni et al. [20], significant velocity fluctuations beyond a critical value during clogging may cause particle bouncing and increase particle penetration by particle re-entrainment.

4. Conclusion

In this study, a methodology for the characterization of velocity patterns in the vicinity of pleated fibrous filters combining experimental and numerical methods has been developed, in the main aim of being able to validate the numerical simulations by local experimental velocity values. The comparison of experimental to numerical velocity values was carried out for a transitional

airflow regime approaching the filter, for which few studies have been reported in the literature. For the CFD calculations the ability of the laminar, standard k-ε and transition SST airflow models to predict the pressure drop and airflow pattern in the vicinity of the filter was thus tested.

If the numerical pressure drop was not significantly affected by the airflow model, the experimental pressure drop was under-predicted by the numerical simulations. It was shown that even slight variations of the pleat dimensions, and modifications of the media properties; especially due to the pleating process in the pleat curved zones; led to non-negligible pressure drop variations. The numerical pressure drop was thus increased by considering the pleats slightly higher and narrower than the mean experimental prototypes dimensions, and by making the extreme hypothesis of impermeable curved pleat zones.

These investigations indicate that for pleat dimensions like those that have been studied (H = 28 mm and W = 25 mm), despite its intrusive character the Hot Wire Anemometry technique is appropriate for velocity acquisitions inside the pleat downstream of the filter, up to a very short distance from the medium surface, and for low velocity values (up to 0.14 $m.s^{-1}$). The comparison of numerical to experimental velocity profiles in the close vicinity of the filter enabled to show that the laminar model was the best for the prediction of the overall airflow pattern. For a transitional airflow regime approaching the filter, and quite "open" pleats, the air velocity was quite homogeneous upstream of the filter, and very close to the mean duct velocity value. The CFD simulations enabled to point out that velocity variations, and more precisely sharp decreases, appeared only in a thin air layer along the medium surface, to reach values close to the theoretical filtration velocity. Significant velocity gradients were observed downstream of the filter and persisted outside the filter.

Another advantage of the HWA anemometry technique is that it also enables to derive turbulence intensity profiles from velocity profiles. The turbulence intensity profiles downstream of the filter showed low variations inside the pleat, and increased outside the pleat. It would be interesting to measure velocity fluctuations for higher filtration velocity values in order to quantify possible fluctuations leading to non-stationary physical phenomena during clogging, such as particle bouncing and re-entrainment.

Acknowledgements

The authors would like to acknowledge the Lydall© Company for supplying the filtering media.

References

[1] C.A. Balaras, A.G. Gaglia, E. Georgopoulou, S. Mirasgedis, Y. Sarafidis, D.P. Lalas, European residential buildings and empirical assessment of the Hellenic building stock, energy consumption, emissions, and potential energy savings, Build. Environ. 42 (2007) 1298–1314.

[2] R.M. Terrill, Laminar Flow in a Uniformly Porous Channel with Large Injection, Aeronaut. Q. 16 (1965) 323–332.

[3] L. Oxarango, P. Schmitz, M. Quintard, Laminar flow in channels with wall suction or injection: a new model to study multi-channel filtration systems, Chem. Eng. Sci. 59 (2004) 1039–1051.

[4] M. Rebaï, M. Prat, M. Meireles, P. Schmitz, R. Baclet, A semi-analytical model for gas flow in pleated filters, Chem. Eng. Sci. 65 (2010) 2835–2846.
[5] S. Fotovati, S.A. Hosseini, H. Vahedi Tafreshi, B. Pourdeyhimi, Modeling instantaneous pressure drop of pleated thin filter media during dust loading, Chem. Eng. Sci. 66 (2011) 4036–4046.
[6] S. Fotovati, H.V. Tafreshi, B. Pourdeyhimi, A macroscale model for simulating pressure drop and collection efficiency of pleated filters over time, Sep. Purif. Technol. 98 (2012) 344–355.
[7] A.M. Saleh, S. Fotovati, H. Vahedi Tafreshi, B. Pourdeyhimi, Modeling service life of pleated filters exposed to poly-dispersed aerosols, Powder Technol. 266 (2014) 79–89.
[8] A.M. Saleh, H.V. Tafreshi, B. Pourdeyhimi, An analytical approach to predict pressure drop and collection efficiency of dust-load pleated filters, Sep. Purif. Technol. 161 (2016) 80–87.
[9] A.M. Saleh, H. Vahedi Tafreshi, A simple semi-numerical model for designing pleated air filters under dust loading, Sep. Purif. Technol. 137 (2014) 94–108.
[10] P.C. Gervais, S. Poussier, N. Bardin-Monnier, G. Karcher, D. Thomas, Combination of Single-Photon Emission and X-Ray Computed Tomography to visualize aerosol deposition in pleated filter, Sep. Purif. Technol. 126 (2014) 52–61.
[11] F. Theron, A. Joubert, L. Le Coq, Numerical and experimental investigations of the influence of the pleat geometry on the pressure drop and velocity field of a pleated fibrous filter, Sep. Purif. Technol. 182 (2017) 69–77.
[12] L. Del Fabbro, J.C. Laborde, P. Merlin, L. Ricciardi, Air flows and pressure drop modelling for different pleated industrial filters, Filtr. Sep. 39 (2002) 34–40.
[13] D.R. Chen, D.Y.H. Pui, B.Y.H. Liu, Optimization of Pleated Filter Designs Using a Finite-Element Numerical Model, Aerosol Sci. Technol. 23 (1995) 579–590.
[14] A.K. Maddineni, D. Das, R.M. Damodaran, Numerical investigation of pressure and flow characteristics of pleated air filter system for automotive engine intake application, Sep. Purif. Technol. 212 (2019) 126–134.
[15] S. Kang, N. Bock, J. Swanson, D.Y.H. Pui, Characterization of pleated filter media using particle image velocimetry, Sep. Purif. Technol. 237 (2020) 116333.
[16] S. Allam, A. Elsaid, Parametric Study on Vehicle Fuel Economy and Optimization Criteria of the Pleated Air Filter Designs to Improve the Performance of an I.C Diesel Engine: Experimental and CFD Approaches, Sep. Purif. Technol. 241 (2020) 116680.
[17] P. Tronville, R. Sala, Minimization of Resistance in Pleated-Media Air Filter Designs: Empirical and CFD Approaches, HVACR Res. 9 (2003) 95–106.
[18] Z. Feng, Z. Long, Q. Chen, Assessment of various CFD models for predicting airflow and pressure drop through pleated filter system, Build. Environ. 75 (2014) 132–141.
[19] G. Lemonis, Three-dimensional measurement of velocity, velocity gradients and related properties in turbulent flows, Aerosp. Sci. Technol. 1 (1997) 453–461.
[20] A.K. Maddineni, D. Das, R.M. Damodaran, Air-borne particle capture by fibrous filter media under collision effect: A CFD-based approach, Sep. Purif. Technol. 193 (2018) 1–10.
[21] A. Zerrouati, M. Rueff, B. Bouchekima, Study of Paper Transverse Shrinkage During Thermal Drying, Dry. Technol. 33 (2015) 1170–1179.
[22] A. Dybbs, R.V. Edwards, A New Look at Porous Media Fluid Mechanics - Darcy to Turbulent, in: J. Bear, M.Y. Corapcioglu (Eds.), Fundam. Transp. Phenom. Porous Media, Springer Netherlands, Dordrecht, 1984 pp. 199–256.